U.S. DEPARTMENT OF ENERGY | Office of Science

DOE/SC-ARM-TR-342
PNNL-39668

Experimental Report: Multi-Instrument Comparison of AAF Size Distribution Instruments

F Mei MS Pekour

July 2026

ARM

DISCLAIMER

This report was prepared as an account of work sponsored by the U.S. Government. Neither the United States nor any agency thereof, nor any of their employees, makes any warranty, express or implied, or assumes any legal liability or responsibility for the accuracy, completeness, or usefulness of any information, apparatus, product, or process disclosed, or represents that its use would not infringe privately owned rights. Reference herein to any specific commercial product, process, or service by trade name, trademark, manufacturer, or otherwise, does not necessarily constitute or imply its endorsement, recommendation, or favoring by the U.S. Government or any agency thereof. The views and opinions of authors expressed herein do not necessarily state or reflect those of the U.S. Government or any agency thereof.

DOE/SC-ARM-TR-342
PNNL-39668

Experimental Report: Multi-Instrument Comparison of AAF Size Distribution Instruments

F Mei
MS Pekour
Both at Pacific Northwest National Laboratory

July 2026

How to cite this document:

Mei, F, and MS Pekour. 2026. Experimental Report: Multi-Instrument Comparison of AAF Size Distribution Instruments. U.S. Department of Energy, Atmospheric Radiation Measurement User Facility, Richland, Washington. DOE/SC-ARM-TR-342.

Work supported by the U.S. Department of Energy,
Office of Science, Office of Biological and Environmental Research

Acronyms and Abbreviations

AAF	ARM Aerial Facility
APS	aerodynamic particle sizer
ARM	Atmospheric Radiation Measurement
DMA	differential mobility analyzer
PCASP	passive cavity aerosol spectrometer probe
POPS	portable optical particle spectrometer
PSL	polystyrene latex
SMPS	scanning mobility particle sizer
UHSAS	ultra-high-sensitivity aerosol spectrometer

Contents

Acronyms and Abbreviations iii
1.0 Introduction 1
2.0 Instrument Description 1
2.1 Sensitivity to Size Ranges 3
2.2 Resolution and Accuracy 3
2.3 Portability and Deployment 3
2.4 Cost and Maintenance 3
3.0 Experimental Setup 3
3.1 Aerosol Generation and Conditioning 5
3.2 PSL Particles for Sizing Measurements and Calibration 5
4.0 Data Analysis and Results 6
4.1 Sizing Accuracy across Instruments 7
4.1.1 POPS Units (x3) 7
4.1.2 UHSAS 10
4.1.3 APS 11
4.1.4 PCASP 12
4.1.5 SMPS 14
4.2 Counting Efficiency across Instruments 15
4.2.1 POPS Units (x3) 17
4.2.2 UHSAS 20
4.2.3 APS 21
4.2.4 PCASP 23
4.2.5 SMPS 25
5.0 Summary 26
5.1 Sizing Accuracy 27
5.2 Counting Efficiency 27
5.3 Inter-POPS Reproducibility 28
5.4 Cross-Instrument Implication 29
6.0 Lessons Learned and Recommendations for Future Deployments 29
7.0 References 30

Figures

1 Experimental setup for size distribution sensors comparison 4
2 Illustration of the size-distribution sensor comparison setup. 4

3 Time series plot of aerosol particle size distribution plot for POPS (434) on May 22, 2026 testing. 5
4 POPS sizing accuracy testing with the PSL nominal size versus sensor measured size for (a) POPS269, (b) POPS308, and (c) POPS434. 9
5 UHSAS sizing accuracy: sensor-measured peak diameter versus nominal PSL diameter for four repeat experiments (13, 15, 18, and 22 May 2026). 11
6 APS sizing accuracy: sensor-measured peak diameter versus nominal PSL diameter for four repeat experiments (13, 15, 18, and 22 May 2026). 12
7 PCASP sizing accuracy: sensor-measured peak diameter versus nominal PSL diameter for four repeat experiments (13, 15, 18, and 22 May 2026). 14
8 SMPS sizing accuracy: sensor-measured peak diameter versus nominal PSL diameter for four repeat experiments (13, 15, 18, and 22 May 2026). 15
9 Averaged number size distributions (dN, non-normalized) measured by all sensors during the 500 nm PSL challenge on 22 May 2026. 16
10 POPS counting efficiency: sensor-reported number concentration (integrated over the relevant peak window) versus the leave-one-out average concentration from all other co-located sensors that have the PSL size within their valid measurement range. (a) POPS269, (b) POPS308, and (c) POPS434. 19
11 UHSAS counting efficiency: sensor-reported number concentration (integrated over the relevant peak window) versus the leave-one-out average concentration from all other co-located sensors that have the PSL size within their valid measurement range. 21
12 APS counting efficiency: sensor-reported number concentration (integrated over the relevant peak window) versus the leave-one-out average concentration from all other co-located sensors that have the PSL size within their valid measurement range. 23
13 PCASP counting efficiency: sensor-reported number concentration (integrated over the relevant peak window) versus the leave-one-out average concentration from all other co-located sensors that have the PSL size within their valid measurement range. 24
14 SMPS counting efficiency: sensor-reported number concentration (integrated over the relevant peak window) versus the leave-one-out average concentration from all other co-located sensors that have the PSL size within their valid measurement range. 26
15 All POPS counting efficiency: sensor-reported number concentration (integrated over the relevant peak window) versus the leave-one-out average concentration from all other co-located sensors that have the PSL size within their valid measurement range. 28

Tables

1 Summary of instrument specifications. 2
2 Test matrix showing data availability 6

1.0 Introduction

Aerosols are particles suspended in the atmosphere, ranging in size from nanometers to micrometers. Their size distribution affects key atmospheric processes, including nucleation, coagulation, scavenging, activation, and radiative properties (Seinfeld and Pandis 2016). Aerosol size distribution is a critical parameter in atmospheric science, influencing processes such as cloud formation and radiative forcing. Accurate representation of aerosol size distributions is essential for understanding their impact on climate, air quality, and human health. However, aerosol size and composition vary significantly across time and space due to meteorological conditions and natural or anthropogenic sources. (Wu and Boor 2021).

Various instruments are used to measure aerosol size distributions, each with distinct principles, advantages, and limitations. This report begins with an in-depth overview of aerosol size-distribution comparison studies, focusing on the passive cavity aerosol spectrometer probe (PCASP), portable optical particle spectrometer (POPS), ultra-high-sensitivity aerosol spectrometer (UHSAS), aerodynamic particle sizer (APS), and scanning mobility particle sizer (SMPS). All of these instruments are used by the U.S. Department of Energy Atmospheric Radiation Measurement (ARM) Aerial Facility (AAF), which commissioned this comparison and report. The report evaluates the strengths and weaknesses of these instruments, highlights their applications, and discusses efforts to merge data from multiple instruments for comprehensive analysis.

2.0 Instrument Description

Aerosol size distribution refers to the quantitative representation of particle sizes within an aerosol sample. It is typically expressed as the number, surface area, or volume of particles per unit size interval. The size distribution is critical for understanding aerosol behavior, including optical properties, chemical reactivity, and health impacts. Aerosol sizes are commonly categorized into three main modes:

- Nucleation Mode: Particles smaller than 0.1 μm, often formed via gas-to-particle conversion processes.
- Accumulation Mode: Particles ranging from 0.1 μm to 2.5 μm, resulting from coagulation or condensation.
- Coarse Mode: Particles larger than 2.5 μm, typically generated by mechanical processes such as dust resuspension or sea spray.

The size distribution is often represented using log-normal distributions, which provide a mathematical framework for describing aerosol populations. Instruments designed to measure aerosol size distributions must account for these modes to provide accurate data.

Aerosol size distribution measurement relies on a variety of instruments, each optimized for specific size ranges, operational principles, and applications. These instruments operate on two primary principles: optical methods (light scattering; e.g., POPS, UHSAS, PCASP) and physical/electrical methods (aerodynamic time-of-flight or electrical mobility; e.g., APS, SMPS). No single instrument spans the entire size range, so researchers often deploy combinations (e.g., SMPS + APS) for comprehensive coverage. Instrument selection depends on the target size range, required resolution, deployment platform

(ground, aircraft, laboratory), type of measurement (laboratory tests versus continues monitoring), cost constraints, and environmental conditions. Key measurement challenges include sensitivity to particle refractive index and shape (optical instruments), hygroscopic growth effects, and the need for regular maintenance and calibration. The key specifications of each instrument are summarized in Table 1.

Table 1. Summary of instrument specifications.

Feature	POPS	UHSAS	APS	SMPS	PCASP
Principle	Light scattering (laser wavelength: 405 nm; light collection angle: 30°-75°)	Light scattering (laser wavelength: 1054 nm; Light collection angle: 33°-147°)*	Aerodynamic time-of-flight	Electrical mobility	Light scattering (laser wavelength: 632.8 nm; Light collection angle: nominally 35°-120°)
Size Range	0.14-3 µm	0.06-1 µm	0.5-20 µm	0.01-1 µm	0.1-3 µm
Type of Size	Optical diameter	Optical diameter	Aerodynamic diameter	Electrical mobility diameter	Optical diameter
# of Bins	100	99	52	64	30
Resolution	Moderate	High	High (coarse mode)	Very high (submicron)	Low
Target Mode	Accumulation	Nucleation / Accumulation	Coarse	Nucleation / Accumulation	Accumulation
Portability	High (compact, lightweight)	Low–Moderate	Low (lab-based)	Low (lab-based)	High (aircraft-mounted)
Deployment	Field / ground-based	Laboratory / field	Laboratory / ground	Laboratory / ground	Airborne (aircraft)
Temporal Resolution	High (real-time)	High (real-time)	High	Low (scanning required)	High (real-time)
Sensitivity to Refractive Index	Yes	Yes	No	No	Yes
Sensitivity to Humidity	Moderate	Moderate	Low	High (drying needed)	Moderate
Sensitivity to Particle Shape	Moderate	Moderate	Low	Low	High
Key Advantage	Portability & low power	Exceptional submicron sensitivity	Accurate coarse-mode sizing	Highest submicron resolution	Robust airborne design
Key Limitation	Limited size range; refractive index dependent	Expensive; contamination by large particles	Ineffective for submicron particles	Long scan times; humidity sensitive	Limited range; shape/composition sensitive

Feature	POPS	UHSAS	APS	SMPS	PCASP
Calibration Needs	Regular	Regular	Regular	Regular	Regular

*Uses two pairs of Mangin optics to collect light across a wide angular range of **33° to 147°**, omitting a central shadowed region between 72.5° and 104.8°.

Each instrument is optimized for specific size ranges, making its selection dependent on the target aerosol population. For example:

2.1 Sensitivity to Size Ranges

- **POPS** and **PCASP** are suitable for accumulation-mode particles, while **APS** excels in coarse-mode measurements.
- **UHSAS** and **SMPS** are ideal for nucleation mode and submicron particles due to their high sensitivity.

2.2 Resolution and Accuracy

- **SMPS** provides the highest resolution for submicron particles, making it indispensable for studies on nucleation and accumulation modes.
- **APS**, while less effective for submicron particles, offers unparalleled accuracy for coarse-mode aerosols.

2.3 Portability and Deployment

- **POPS** and **PCASP** are highly portable and suitable for field and airborne measurements, respectively.
- Instruments like **SMPS** and **APS** are more suited for laboratory or ground-based environments due to their size and operational requirements.

2.4 Cost and Maintenance

- **UHSAS** and **SMPS** are expensive but offer high precision and resolution.
- **POPS** and **APS** are more cost-effective but require regular calibration to maintain accuracy.

3.0 Experimental Setup

Figures 1 and 2 depict the experimental setup employed in this intercomparison study. The system was engineered to supply a well-characterized, monodisperse aerosol consisting of polystyrene latex (PSL) particles simultaneously to all instruments under evaluation, thereby facilitating an equitable and consistent comparison of size distribution measurements. At each specified aerosol-testing size, PSL particles were generated for a duration of 20 minutes, as detailed in Figure 3. When transitioning between

different PSL particle sizes, the chamber was flushed with filtered air to maintain integrity. Four replicate experiments conducted on 13, 15, 18, and 22 May 2026 further reinforced the assessment by indicating whether observed biases were systematic or specific to certain days.

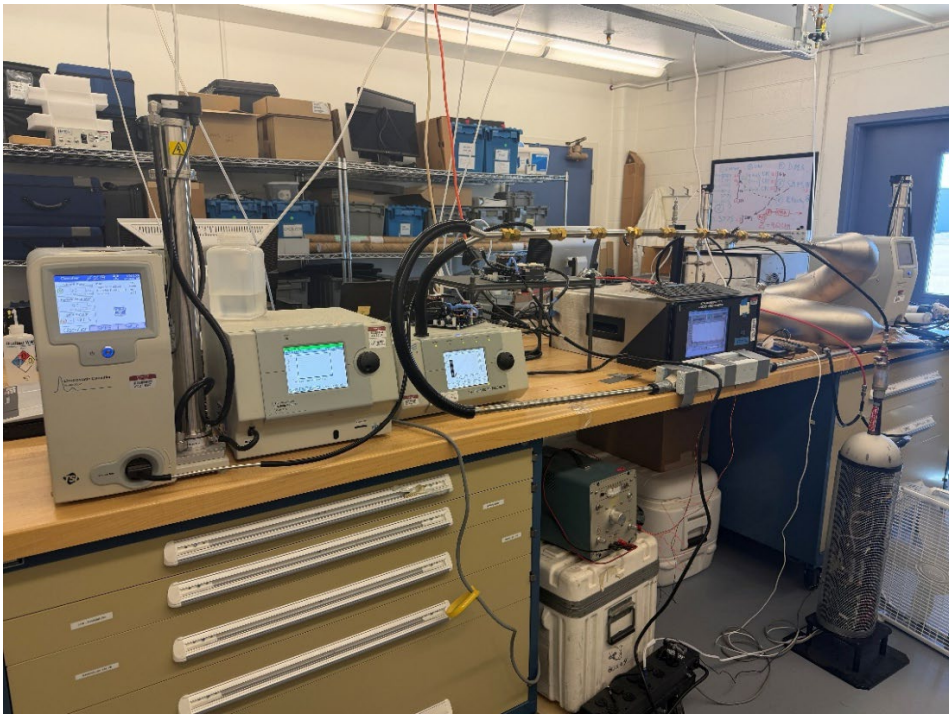


Figure 1. Experimental setup for size distribution sensors comparison.

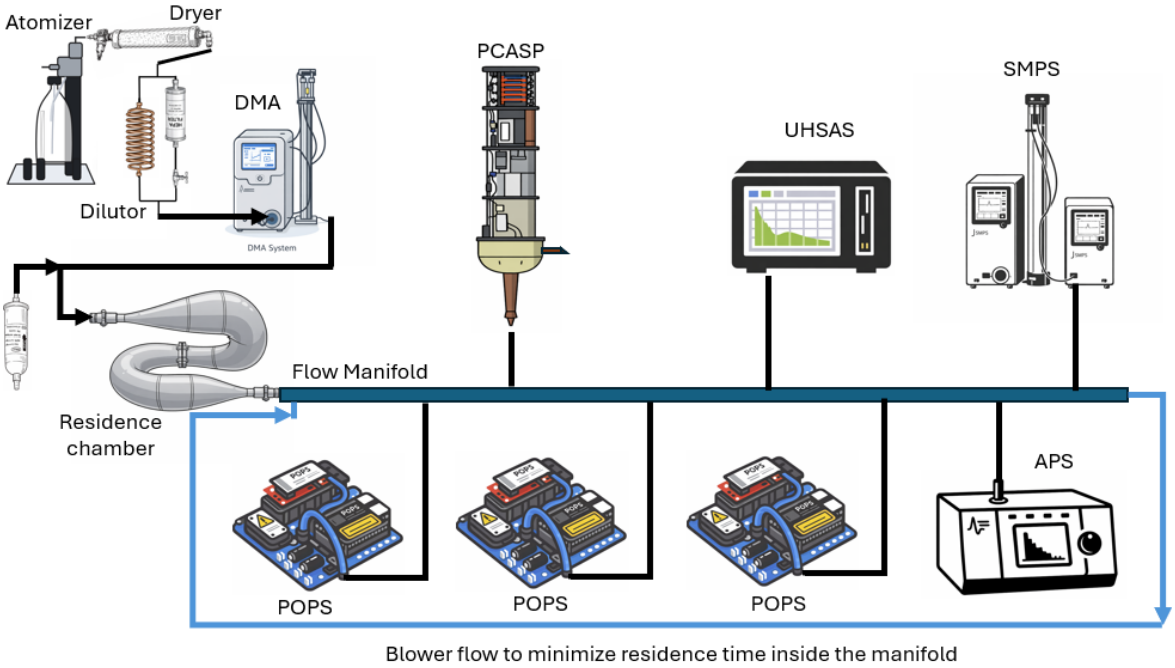


Figure 2. Illustration of the size-distribution sensor comparison setup.

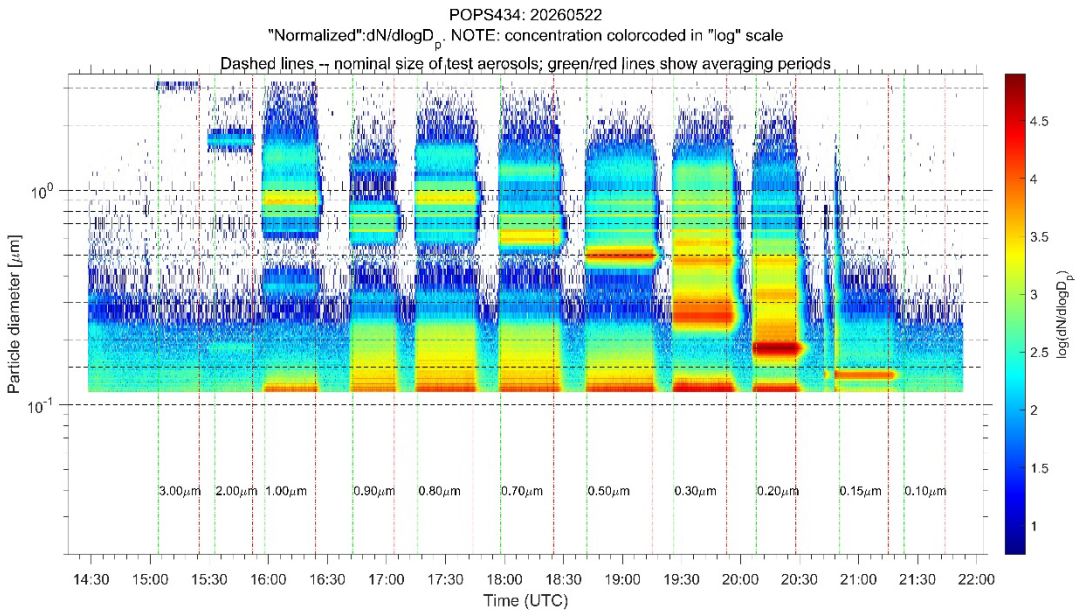


Figure 3. Time series plot of aerosol particle size distribution plot for POPS (434) on May 22, 2026 testing.

3.1 Aerosol Generation and Conditioning

Polydisperse aerosol particles were generated using an atomizer with a diluted suspension of certified PSL particles. The air was "pushed" through the atomizer to ensure delivery of polydisperse aerosol to a differential mobility analyzer (DMA) at a specific flow rate. For smaller sizes (below 200 nm), the atomizer output was dried and passed through a diluter before being directed into the DMA, which selected particles with a specific electrical mobility diameter, producing a monodisperse aerosol stream. The size-selected aerosol was then passed through a residence chamber to stabilize the flow and ensure the particle concentration became spatially uniform before reaching the instruments.

The conditioned aerosol exiting the residence chamber was introduced into a common sampling manifold (a ¾-inch tubing with multiple pickup points (1/4 inch) along the sampling line). This manifold was designed to evenly distribute the aerosol to all instruments simultaneously, minimizing concentration gradients and particle losses across the sampling ports. An additional blower was installed to circulate air through the manifold and back to the residence chamber, thereby improving mixing and minimizing time delays in the aerosol transport.

3.2 PSL Particles for Sizing Measurements and Calibration

PSL particles are widely recognized as the gold standard for calibrating particle sizing instruments due to their highly spherical morphology, exceptional monodispersity, and chemical stability. Produced through the emulsion polymerization of styrene, these particles are available in precisely controlled diameters ranging from approximately 20 nm to several millimeters, with sizing accuracies on the order of 0.01 µm. The sizes we used in this study are 100±3 nm, 152±5 nm, 203±5 nm, 303±6 nm, 510±7 nm, 707±9 nm, 799±9 nm, 903±12 nm, 0.99±0.03 µm, 1.93± µm, and 3.00±0.07 µm. Their narrow size distributions and well-characterized refractive index (approximately 1.57-1.62) make them ideal reference materials for

calibrating aerosol optical particle counters, laser diffraction systems, surface scanning inspection systems, and electron microscopes. In practice, PSL spheres are typically supplied as aqueous suspensions and can be aerosolized or deposited onto substrates to verify instrument response across a range of particle diameters. Because their optical and physical properties are highly reproducible from lot to lot, PSL standards enable traceable, repeatable measurements that ensure compliance with metrology requirements in semiconductor manufacturing, pharmaceutical cleanroom monitoring, and environmental particulate analysis.

4.0 Data Analysis and Results

This section presents the data-processing methodology and a comparative analysis of size-distribution measurements obtained from seven instruments: three POPS units, one UHSAS, one APS, one PCASP, and one SMPS. Each instrument was challenged with monodisperse PSL particles spanning two orders of magnitude in diameter (100 nm to 3 μm), with the smallest two sizes (100 nm and 152 nm) additionally cleaned via DMA selection and the remaining sizes produced from certified PSL suspensions. The analysis focuses on two key performance metrics: (1) sizing accuracy, evaluated by comparing each instrument's reported peak diameter against the nominal PSL diameter (session 4.1), and (2) counting efficiency, evaluated using a leave-one-out reference concentration derived from the ensemble of co-located sensors (session 4.2). More discussion was included in the 4.1 and 4.2 sessions. Because the instruments differ in measurement principle — optical scattering (POPS, UHSAS, PCASP), aerodynamic time-of-flight (APS), and electrical mobility (SMPS) — and in their nominal operating size ranges, not every instrument is expected to detect every test particle. Establishing the valid measurement domain for each instrument is, therefore, the necessary first step before any quantitative comparison can be made. It should be noted that the optical-based instruments and the APS are normally calibrated with PSLs, so no “refractive index” or “density” adjustments were applied in the data processing.

Table 2 summarizes the test matrix and indicates, for each combination of nominal PSL size and instrument, whether the particle falls within the instrument's specified detection range. Sizes marked with a checkmark (✓) lie comfortably within the manufacturer-specified range and are included in the subsequent sizing accuracy and counting efficiency analyses. Entries marked with a tilde (~) indicate sizes near the upper or lower detection limit, where reduced bin resolution or declining detection efficiency may bias the measurement; results from these points are reported but interpreted with caution. Crosses (✗) denote sizes outside the instrument's operating range, for which no data are reported. This matrix defines the subset of instruments contributing to the leave-one-out reference at each PSL size and frames the cross-instrument comparisons presented in the remainder of this section.

Table 2. Test matrix showing data availability.

PSL Size	Nominal Size	POPS269	POPS308	POPS433	UHSAS	APS	PCASP	SMPS
100± 3 nm	100 nm (DMA)	~	~	~	✓	✗	✓	✓
152±5 nm	152 nm (DMA)	✓	✓	✓	✓	✗	✓	✓
203±5 nm	203 nm	✓	✓	✓	✓	✗	✓	✓
303±6 nm	303 nm	✓	✓	✓	✓	✗	✓	~

PSL Size	Nominal Size	POPS269	POPS308	POPS433	UHSAS	APS	PCASP	SMPS
510±7 nm	510 nm	✓	✓	✓	✓	✓	✓	✗
707±9 nm	707 nm	✓	✓	✓	✓	✓	✓	✗
799±9 nm	799 nm	✓	✓	✓	✓	✓	✓	✗
903±12 nm	903 nm	✓	✓	✓	✓	✓	✓	✗
0.99±0.03 µm	0.99 µm	✓	✓	✓	~	✓	✓	✗
1.93± 0.06 µm	1.93 µm	✓	✓	✓	✗	✓	✓	✗
3.00±0.07 µm	3.00 µm	~	~	~	✗	✓	✓	✗

4.1 Sizing Accuracy across Instruments

Sizing accuracy was evaluated by comparing each instrument's measured peak diameter to the nominal PSL diameter across the test matrix defined in Table 2. For every PSL challenge, the “relevant” peak edges are defined by a level of 50% from the peak maximum. The following subsections present the measured-versus-nominal diameter plots for each sensor, beginning with the three POPS units to assess unit-to-unit reproducibility, followed by the UHSAS, APS, PCASP, and SMPS. For each instrument, deviations (10% and 20%) from the 1:1 line are shown on the plots and discussed.

4.1.1 POPS Units (x3)

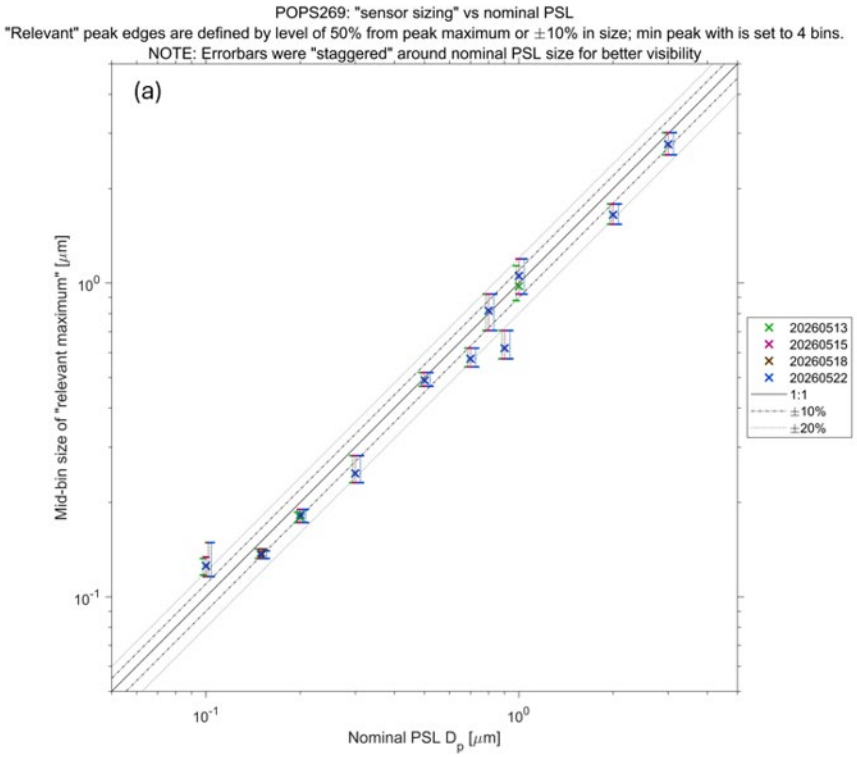
Figure 4(a-c) shows the sizing response of POPS269, POPS308, and POPS434 across the full PSL test range (100 nm to 3 µm) for four repeat experiments conducted on 13, 15, 18, and 22 May 2026. For each PSL challenge, the marker indicates the mid-bin diameter corresponding to the averaged peak maximum, and the error bars span the “relevant” peak edges, defined as the bin diameters at which the count drops to 50% of the peak maximum (or ±10% in size, whichever is wider, with a minimum peak width of four bins). Reference lines indicate the 1:1 agreement and the ±10% and ±20% deviation envelopes. (Mei et al. 2020)

Across the full test range, all POPS demonstrate good sizing accuracy and excellent day-to-day reproducibility: the four repeat measurements at each nominal PSL size are nearly indistinguishable, with all markers overlapping within the symbol size. The sensor's measured peak diameter agrees with the nominal PSL size to within ±20% across nearly the entire range, and to within ±10% for most sizes between 200 nm and 2 µm. Several size-dependent features merit attention:

- **Small-particle end (100-150 nm):** The reported peak diameters lie slightly above the 1:1 line, falling near the +20% envelope at 100 nm. This behavior is consistent with operation near the lower detection limit of the POPS (~135 nm), where bin resolution is coarse, and the lowest detectable bin biases the reported peak diameter upward.
- **Mid-range (200-500 nm):** Measurements track the 1:1 line closely, generally within ±10%, indicating reliable sizing in this range.

- **Mie-resonance region (700-1000 nm):** A systematic underestimation is observed, with measured diameters falling below the 1:1 line and approaching the -20% envelope near 800-900 nm. This deviation is characteristic of optical particle counters operating with a 405 nm laser, where the non-monotonic relationship between scattering cross-section and particle diameter (Mie resonances) causes ambiguity in the size-to-signal mapping for particles whose diameter is comparable to the laser wavelength.
- **Super-micron range (2-3 µm):** The sensor recovers good agreement with the nominal size, returning to within ±10% of the 1:1 line.

The error bars (peak edges at 50% of maximum) are also informative: they are narrowest in the mid-range and widen at both ends of the size range, reflecting the coarser bin spacing at the detection limits and the broader scattering response in the Mie-resonance region. Overall, POPS exhibits stable, reproducible sizing performance that is well characterized by the expected optical-sizing behavior of a 405 nm scattering instrument, with the largest deviations confined to the Mie-resonance region near 800-900 nm.



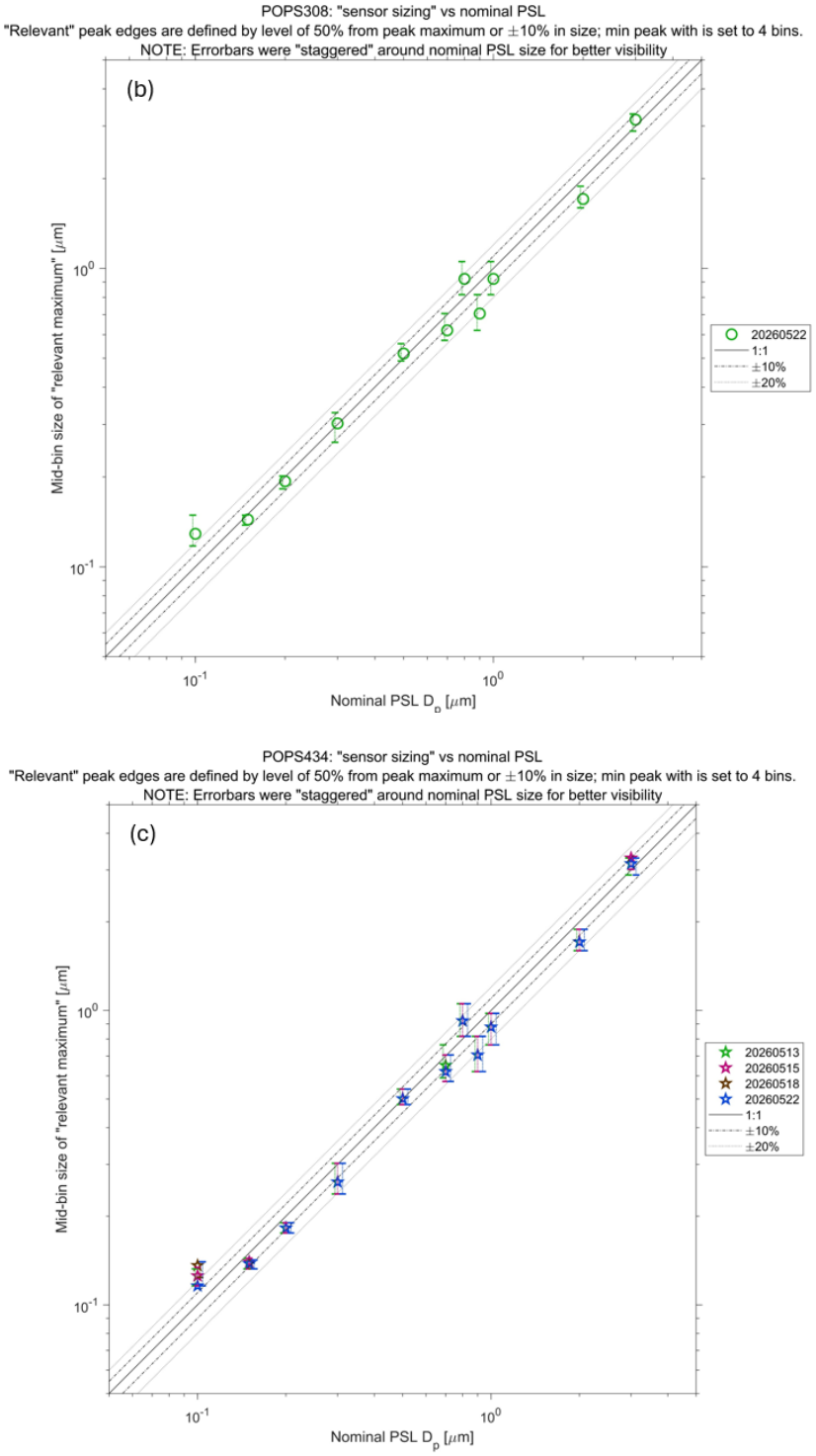


Figure 4. POPS sizing accuracy testing with the PSL nominal size versus sensor measured size for (a) POPS269, (b) POPS308, and (c) POPS434. Note that POPS308 is available only on the last day of testing on May 22, 2026.

4.1.2 UHSAS

Similar to the POPS plot, Figure 5 shows the sizing response of the UHSAS across the PSL test range for the four repeat experiments conducted on 13, 15, 18, and 22 May 2026. Data are presented only up to ~1 μm, consistent with the UHSAS's upper detection limit; the 2 μm and 3 μm PSL challenges fall outside the instrument's specified range and are not reported.(Kupc et al. 2018)

Across its operating range, the UHSAS exhibits excellent sizing accuracy and very high day-to-day reproducibility:

- **Small-particle end (100-150 nm): The** reported peak diameters lie essentially on the 1:1 line, well within ±10% of the nominal size. This is a notable advantage of the UHSAS over the 405 nm POPS at this end of the range — the high-power 1054 nm laser combined with two stage photodetector system account for fine bin resolution of the UHSAS and accurate sizing of sub-200 nm PSL particles without the upward bias seen near the POPS detection limit.
- **Mid-range (200-500 nm):** Measurements track the 1:1 line very closely, with all four repeats falling inside the ±10% envelope. Error bars are narrow, indicating well-resolved, sharply peaked size distributions.
- **Upper range (700-1000 nm):** A small but systematic underestimation appears, with measured diameters falling slightly below the 1:1 line and approaching the -10% envelope near 800-1000 nm. This is consistent with the onset of Mie-resonance ambiguity as the particle diameter approaches the UHSAS laser wavelength (1054 nm), as well as the reduced bin resolution near the upper end of the instrument's range. The deviation, however, remains substantially smaller than that observed for the POPS units in the same size region, because the longer UHSAS wavelength shifts the strong Mie oscillations to larger particle sizes.

The error bars (peak edges at 50% of maximum) are uniformly narrow across the full range, reflecting the high size resolution of the UHSAS (~99 bins) and the sharpness of the measured PSL peaks. Repeatability across the four test days is excellent, with the four markers at each nominal size overlapping within the symbol size.

Overall, the UHSAS demonstrates the best sizing accuracy among the optical instruments tested, with measurements agreeing with nominal PSL diameters to within ±10% across its full operational range, and only minor deviations appear near 1 μm, where Mie-resonance effects begin to influence the sizing response.

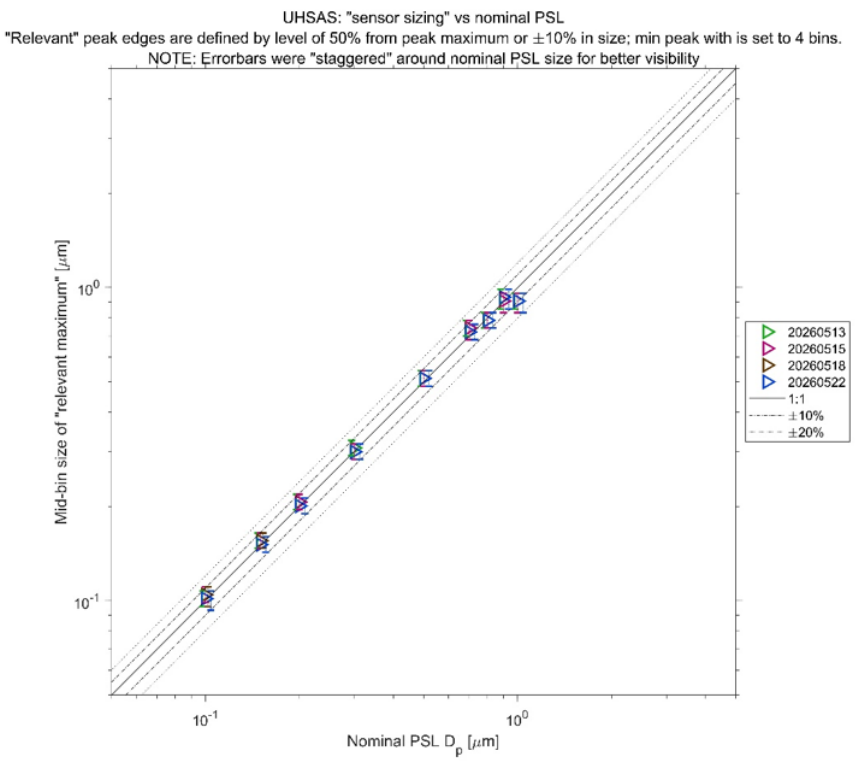


Figure 5. UHSAS sizing accuracy: sensor-measured peak diameter versus nominal PSL diameter for four repeat experiments (13, 15, 18, and 22 May 2026).

4.1.3 APS

Figure 6 shows the sizing response of the APS across the PSL test range for the four repeat experiments conducted on 13, 15, 18, and 22 May 2026. Data are presented from 500 nm upward, consistent with the lower detection limit of the APS; the 100 nm, 150 nm, 200 nm, and 300 nm PSL challenges fall outside the instrument's specified range and are not reported. (Johnson et al. 2018)

Across its operating range, the APS exhibits good day-to-day reproducibility — the four repeat measurements at each nominal size overlap closely — but the reported peak diameters are systematically biased low relative to the nominal PSL size:

- **Lower range (500-700 nm):** The measured peak diameters fall well below the 1:1 line, exceeding the -20% deviation envelope. At 500 nm and 700 nm the offset corresponds to roughly one to two APS bins, which, given the logarithmic bin spacing of the APS (32 channels per decade), translates to a ~6-13% downward shift per bin. The observed offset is therefore consistent with a one- to two-bin systematic shift in the reported diameter.
- **Mid-range (800-1000 nm):** The bias is reduced but still present, with measurements falling between the -10% and -20% envelopes. Reproducibility across the four test days remains excellent.
- **Super-micron range (2-3 µm):** The systematic underestimation persists, with measured diameters near the -20% envelope at 3 µm.

The APS reports aerodynamic diameter rather than physical (geometric) diameter. However, for PSL spherical particles with a density of nearly 1 g/cc, aerodynamic diameter is the same as geometric one. The offset of one to two bins across the full size range suggests a calibration or bin-edge assignment issue in the APS sizing channel, rather than a physical measurement effect. A similar one-to-two-bin low bias for PSL has been reported in the literature for the APS 3321 and is commonly attributed to particle-orientation effects during acceleration and to the sensitivity of the time-of-flight inversion to the assumed Stokes correction.

The error bars are noticeably wider than UHSAS, particularly at 500-700 nm, where the lower edge of the relevant peak window extends well below the marker. This reflects coarser bin structure and the broader response function of the APS near its lower size limit, where the time-of-flight signal-to-noise degrades, and the measured peaks become asymmetric.

Overall, the APS provides reproducible measurements but consistently undersizes PSL particles by approximately one to two bins (~10-20%) across its full operating range.

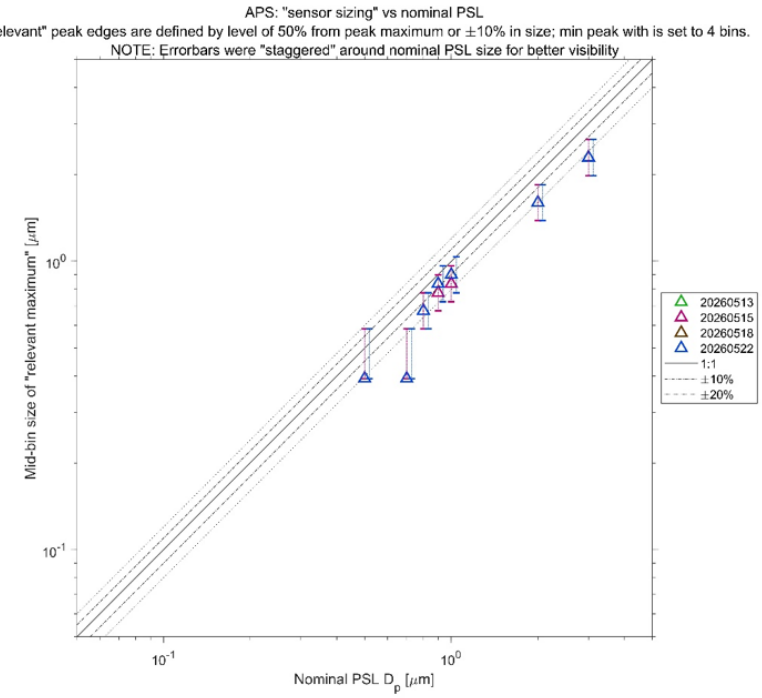


Figure 6. APS sizing accuracy: sensor-measured peak diameter versus nominal PSL diameter for four repeat experiments (13, 15, 18, and 22 May 2026).

4.1.4 PCASP

Figure 7 shows the sizing response of the PCASP across the full PSL test range (100 nm to 3 μm) for the four repeat experiments conducted on 13, 15, 18, and 22 May 2026. The most prominent feature of the PCASP results is the wide error bars observed across nearly the entire size range. Unlike the UHSAS, whose error bars are typically narrower than the marker symbols, the PCASP error bars frequently span ±20% or more around the reported peak diameter. This is a direct consequence of the PCASP's coarse bin structure: with only ~30 channels distributed across its full size range (~100 nm to 3 μm), the bin width

near each PSL test size is large, and the peak edges at 50% of maximum frequently extend across one or two adjacent bins on each side. The four-bin minimum peak-width criterion further widens the reported error bars at sizes where the true PSL response is contained within only one or two bins. (Reid et al. 2003)

Despite the limited size resolution, the PCASP demonstrates reasonable sizing accuracy and good day-to-day reproducibility:

- **Small-particle end (100-200 nm):** The reported peak diameters lie close to the 1:1 line, generally within the ±10% envelope. One outlier is observed at 150 nm on 18 May 2026, where the measurement falls below the -20% envelope; this is likely the result of the peak being contained within a single bin near the lower detection limit, where the fitted mid-bin diameter is highly sensitive to the bin-edge assignment.
- **Mid-range (300-700 nm):** Measurements track the 1:1 line within the ±10% envelope. Error bars remain wide owing to the coarse bin spacing, but the central marker positions are consistent across the four test days.
- **Mie-resonance region (800-1000 nm):** A modest underestimation is observed, with measured diameters falling between the -10% and -20% envelopes. This behavior is qualitatively similar to that observed for the POPS and UHSAS in the same-size region and is consistent with the well-known Mie-resonance ambiguity in optical particle counters.
- **Super-micron range (2-3 µm):** Sizing recovers to within ±10% of the 1:1 line, with reproducible markers across the four test days.

We emphasize that the wide error bars reported here primarily reflect the instrument's intrinsic size bin structure rather than measurement noise or run-to-run variability. The marker positions themselves (the mid-bin diameters of the peak maxima) are highly reproducible across the four test days, indicating that the PCASP responds consistently to a given PSL size — its limitation lies in the coarseness with which that size is reported, not in the stability of the measurement.

Overall, the PCASP provides reliable sizing within ±20% of the nominal PSL diameter across the full test range, with reproducibility comparable to the higher-resolution optical instruments. However, its coarse bin structure makes it less suitable than the POPS or UHSAS for applications requiring fine-scale size discrimination, particularly in the sub-micron range, where the PCASP bin widths are largest relative to particle diameter.

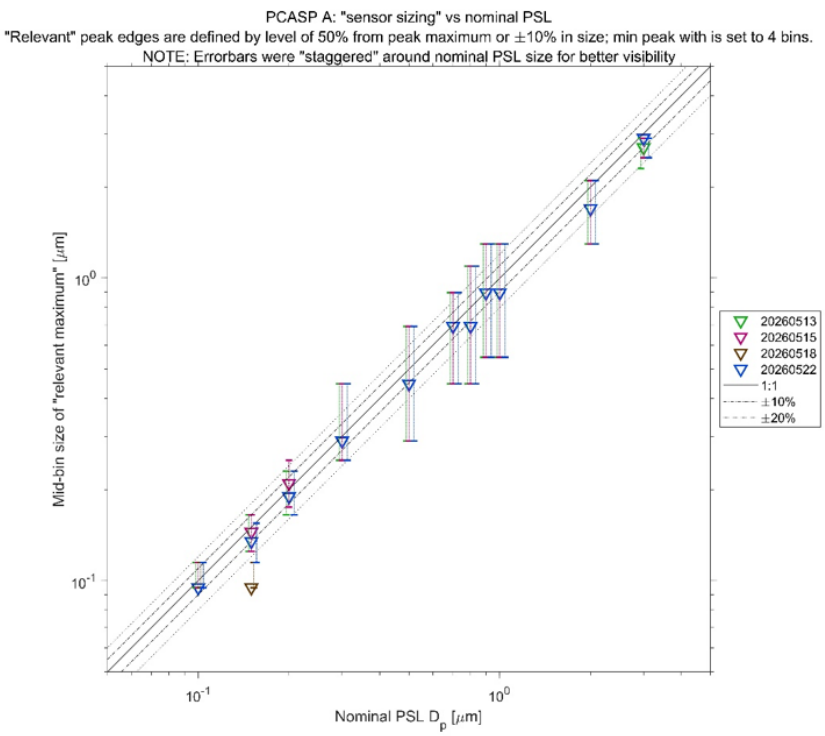


Figure 7. PCASP sizing accuracy: sensor-measured peak diameter versus nominal PSL diameter for four repeat experiments (13, 15, 18, and 22 May 2026).

4.1.5 SMPS

Figure 8 shows the sizing response of the SMPS for the four repeat experiments conducted on 13, 15, 18, and 22 May 2026. Data are presented only for nominal PSL diameters of 100, 150, 200, and 300 nm. Although the SMPS is nominally capable of measurements up to ~1 μm, the upper size limit achievable in this experiment was constrained by the operating configuration: the atomizer delivered an aerosol flow of 2.5 LPM, and the corresponding sheath-to-aerosol flow ratio required to scan to larger sizes would have either exceeded the DMA's allowable sheath flow range or compromised the size-selection resolution. Balancing these two constraints, ~300 nm represents the largest PSL diameter for which the SMPS could provide a well-resolved scan, and PSL particles larger than 300 nm are therefore not reported. (Stolzenburg 1988)

Within the achievable size range, the SMPS demonstrates excellent sizing accuracy and very good day-to-day reproducibility:

- **100 nm and 300 nm:** The reported peak diameters lie essentially on the 1:1 line, with all four repeat measurements falling well within the ±10% envelope. Error bars are narrow, reflecting the high mobility resolution of the DMA at sub-200 nm sizes.

We emphasize that, because the SMPS reports electrical-mobility diameter, it serves as the most direct and physically traceable size reference among the instruments tested in this study, particularly for the sub-300 nm range. The agreement between the SMPS-reported diameters and

the nominal PSL sizes, within ±10% across the full achievable range, provides confidence in both the SMPS calibration and the nominal PSL sizes. This makes the SMPS a valuable benchmark for evaluating the sizing performance of the optical instruments in the overlapping 100-300 nm range, where the POPS and PCASP exhibited their largest deviations.

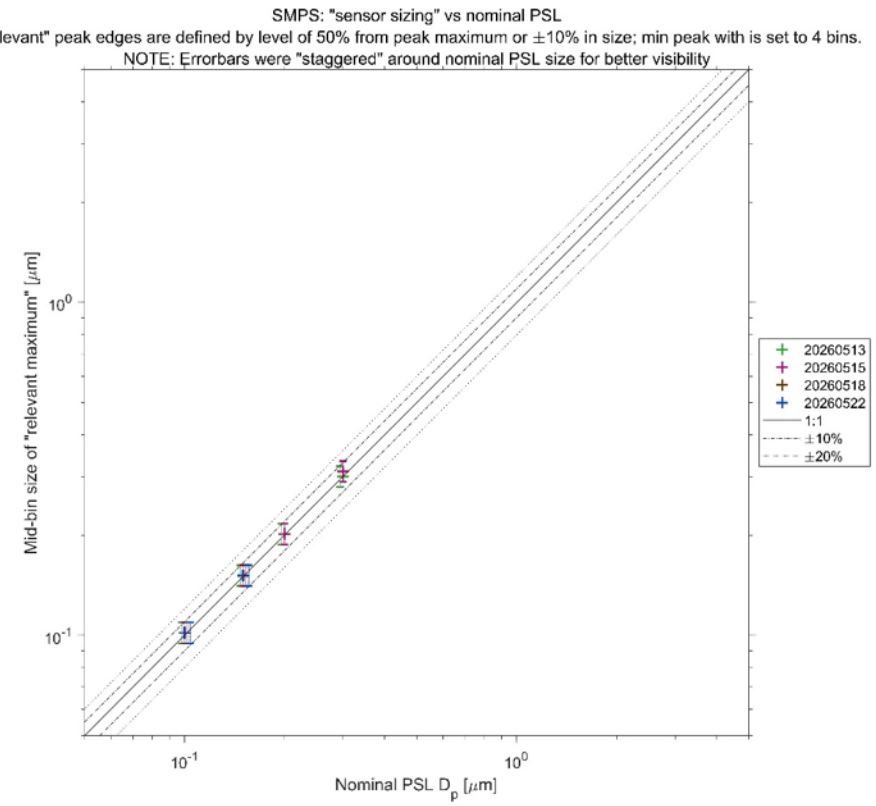


Figure 8. SMPS sizing accuracy: sensor-measured peak diameter versus nominal PSL diameter for four repeat experiments (13, 15, 18, and 22 May 2026).

4.2 Counting Efficiency across Instruments

For each PSL size, the number concentration reported by each sensor was estimated by integrating the measured size distribution over the "relevant" peak window — the same window used in the sizing-accuracy analysis. Specifically, the peak maximum was first identified in the averaged size distribution (in non-normalized dN form) for the steady-state sampling period, and the relevant peak edges were defined as the bin diameters at which the response falls to 50% of the peak maximum (or ±10% in size, whichever is wider, subject to a minimum peak width of four bins). The sensor-reported number concentration for that PSL size was then computed as the sum of the bin counts within these peak edges:

$$N_{\text{sensor}} = \sum_{i \in \text{peak window}} N_i$$

This approach isolates the contribution of the target PSL particles from background aerosol, multi-charged satellite peaks (for DMA-selected sizes), and PSL residual/surfactant artifacts at smaller diameters, all of which appear as secondary features in the measured distributions. As an example, Figure 9 shows the averaged size distributions from all sensors for the 500 nm PSL challenge on 22 May 2026, with the markers indicating the integration window used for each instrument. The integrated counts and mid-bin peak diameters are reported in the legend (e.g., POPS269: N = 444.0 cm^{-3}, Dp = 0.49 µm; UHSAS: N = 359.9 cm^{-3}, Dp = 0.51 µm; APS: N = 401.7 cm^{-3}, Dp = 0.39 µm), and the dashed vertical line marks the nominal PSL diameter. The use of an instrument-specific peak window — rather than a single, fixed-size range applied uniformly across all sensors — ensures that each instrument's reported concentration reflects its own response to the PSL peak, accommodating the different bin structures, sizing biases, and resolution characteristics documented in Section 4.1.

The counting efficiency for each sensor at each PSL size was then evaluated using a leave-one-out reference: for a given sensor, the reference concentration is taken as the average of the integrated counts from all *other* sensors that have the PSL size within their valid measurement range (per Table 2):

$$\mathrm{CE}_j = \frac{N_{\mathrm{sensor},j}}{\langle N_{\mathrm{sensor},k} \rangle_{k \neq j}}$$

This leave-one-out approach provides an empirical reference independent of any single instrument's calibration while making maximum use of the redundancy among the other co-located sensors. Sensors for which the PSL size lies outside their valid range (e.g., APS for 100-300 nm, SMPS for ≥500 nm in this experiment) are excluded from both the numerator and the denominator at that size, ensuring that each leave-one-out reference is computed only from instruments expected to detect the target particle.

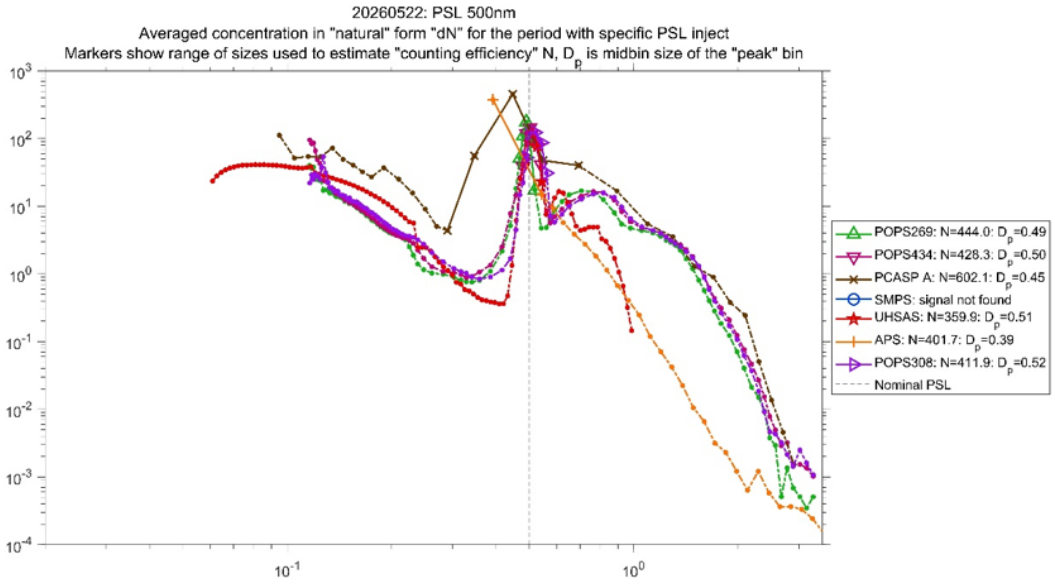


Figure 9. Averaged number size distributions (dN, non-normalized) measured by all sensors during the 500 nm PSL challenge on 22 May 2026. Markers indicate the "relevant" peak window — the bin range used to estimate the integrated number concentration for each sensor. The dashed vertical line indicates the nominal PSL diameter. Legend entries report the integrated number concentration, N (cm^{-3}), and the mid-bin peak diameter, Dp (µm), for each sensor.

4.2.1 POPS Units (x3)

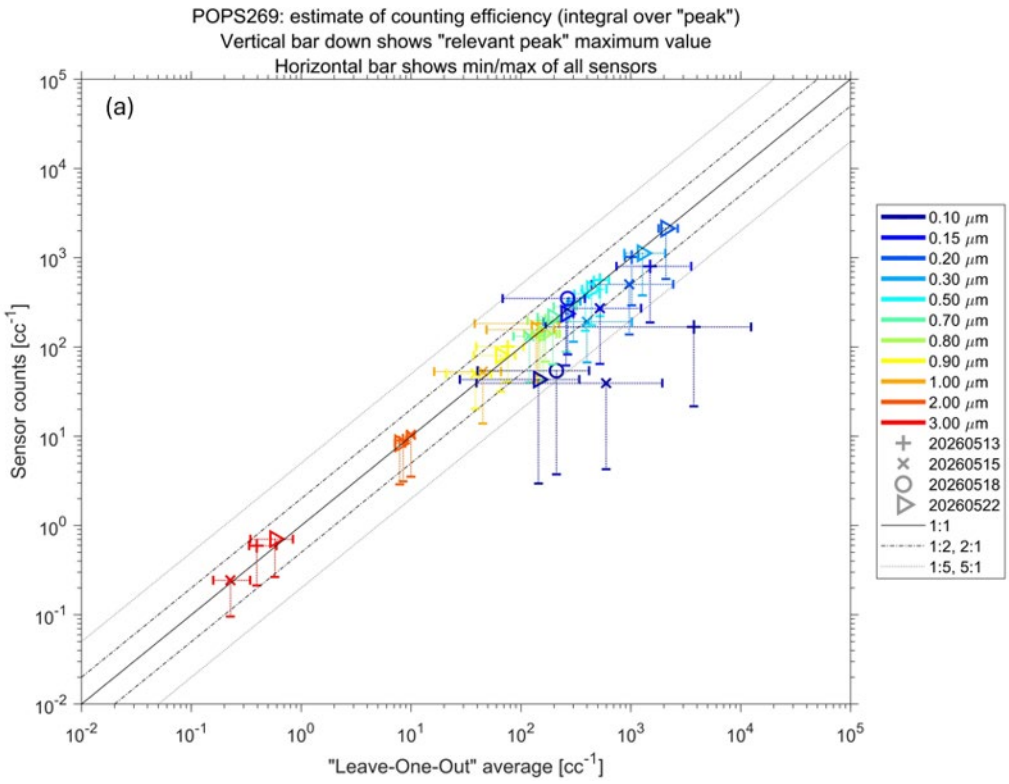
Figure 10 (a-c) shows the counting-efficiency response of POPS269, POPS308, and POPS434 across the full PSL test range (100 nm to 3 μm) for the four repeat experiments conducted on 13, 15, 18, and 22 May 2026. The sensor-reported number concentration (integrated over the relevant peak window, as described in Section 4.2) is plotted against the leave-one-out average concentration from all other co-located sensors that have the corresponding PSL size within their valid measurement range. Marker color denotes the nominal PSL diameter, and marker shape denotes the test date. The vertical bar (downward) indicates the maximum bin value within the relevant peak, and the horizontal bar shows the minimum and maximum leave-one-out values across the contributing sensors. Reference lines indicate 1:1 agreement and the 1:2/2:1 and 1:5/5:1 deviation envelopes. (Mei et al. 2020)

Across most of the test range, POPS tracks the leave-one-out reference within a factor of two, demonstrating reasonable counting agreement with the ensemble of co-located sensors. Several size-dependent features are evident:

- **Sub-200 nm range (100 nm and 150 nm):** The counting efficiency is markedly reduced. The 100 nm and 150 nm markers consistently fall below the 1:1 line, with several points near or beyond the 1:5 envelope. This behavior is the direct consequence of operating below the specified lower detection limit of the POPS (~135 nm): at 100 nm, the PSL particles are entirely below the detection threshold, and only a small fraction is registered owing to the finite tail of the detection-efficiency curve and possible contributions from the multiply-charged satellite particles (which are larger than the DMA-selected primary mode). At 150 nm, the particles lie just above the nominal cutoff, where the detection efficiency is rising steeply but has not yet reached unity; the resulting counts are therefore variable and significantly below the leave-one-out reference, which is dominated by the UHSAS and SMPS — both of which fully detect particles in this size range. The wide vertical and horizontal error bars in this range also reflect the sensitivity of the integrated counts to bin-edge placement when the peak straddles the lower detection limit.
- **Mid-range (200-500 nm):** The markers cluster tightly around the 1:1 line, generally within the 1:2/2:1 envelope. POPS is well within its specified operational range here, and the counting agreement with the leave-one-out reference is good. Day-to-day reproducibility across the four test markers is also strong.
- **Mie-resonance region (700-1000 nm):** Counts continue to track the 1:1 line within a factor of two, although the scatter is somewhat larger than in the mid-range. The slightly broadened response in this region — already noted in the sizing-accuracy analysis (Section 4.1.1) — leads to a wider integration window and contributes to the larger spread in the integrated counts.
- **Super-micron range (2-3 μm):** Although the absolute concentrations are very low (typically <10 cm^{-3}), POPS again tracks the leave-one-out reference within a factor of two, with the four test days clustering around the 1:1 line. The wider relative scatter in this range is consistent with counting-statistics noise at low concentrations rather than a systematic instrument bias.

Overall, all POPS demonstrate good counting agreement with the leave-one-out reference across their specified operating range, with a clear and physically expected loss of counting efficiency below ~150 nm associated with their lower detection limit. The deviations observed at 100 nm and 150 nm should not be interpreted as a measurement defect but rather as a fundamental optical sensitivity limit of the POPS for sub-detection-limit particles. For applications targeting particles below ~200 nm, this lower-limit

behavior must be accounted for, and the POPS counts should be supplemented by a sensor with sub-150 nm sensitivity (such as the UHSAS or SMPS).



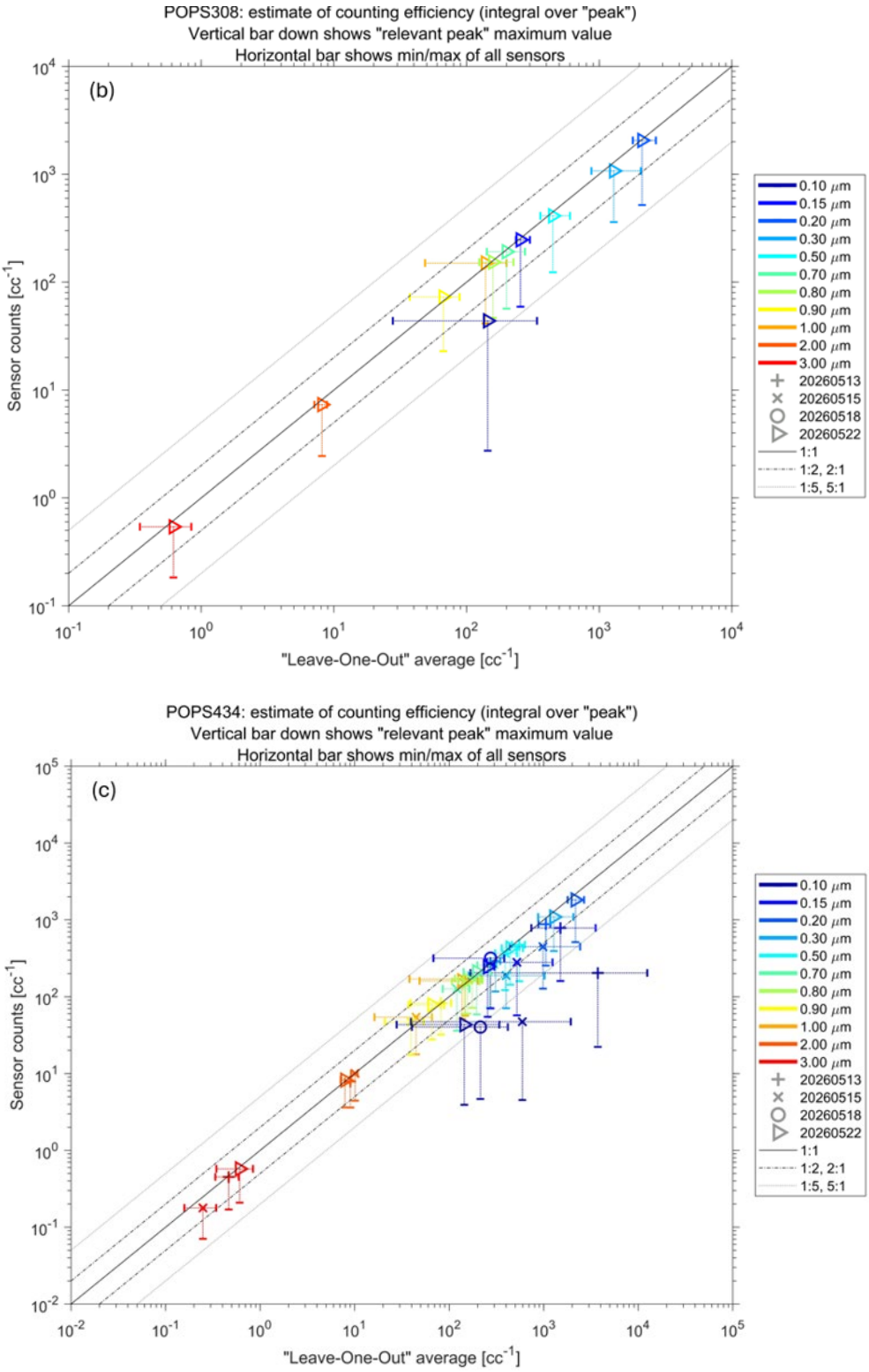


Figure 10. POPS counting efficiency: sensor-reported number concentration (integrated over the relevant peak window) versus the leave-one-out average concentration from all other co-located sensors that have the PSL size within their valid measurement range. (a) POPS269, (b) POPS308, and (c) POPS434.

4.2.2 UHSAS

Figure 11 shows the counting-efficiency response of the UHSAS across its operational PSL test range (100 nm to 1 μm) for the four repeat experiments conducted on 13, 15, 18, and 22 May 2026. Data are not reported for PSL diameters above 1 μm, which are outside the UHSAS detection range.
(Kupc et al. 2018) The UHSAS counting-efficiency response exhibits a clear size-dependent pattern, with good agreement with the leave-one-out reference at small sizes and a progressive undercount at larger sizes:

- **Sub-200 nm range (100 nm and 150 nm):** The UHSAS markers cluster tightly around the 1:1 line, generally within the 1:2/2:1 envelope. This is consistent with the high sub-200 nm sensitivity of the UHSAS (1054 nm laser, ~55 nm lower detection limit) and confirms the UHSAS's role as one of the dominant sensors contributing to the leave-one-out reference at these sizes (the others being the SMPS and PCASP). The wide horizontal error bars at 100 nm reflect the substantial sensor-to-sensor disagreement among the contributing instruments at this challenging size, rather than a UHSAS measurement issue.
- **Mid-range (200-500 nm):** Markers track the 1:1 line within the 1:2/2:1 envelope, with good day-to-day reproducibility across the four test markers. This is the optimal operating range for the UHSAS, where it is well within both its detection limit and its high size-resolution range.
- **Upper range (700-1000 nm):** A systematic undercount develops, with the markers progressively dropping below the 1:1 line. By 900 nm and 1 μm, several measurements approach or fall below the 1:5 envelope. The leave-one-out reference at these sizes is dominated by the POPS units, the PCASP, and the APS, all of which agree within a factor of two with each other in this region (per Sections 4.2.1, 4.2.3, and 4.2.4); the UHSAS therefore appears to be the discrepant sensor at the upper end of its range.

The systematic UHSAS undercount above ~700 nm is likely explained by the size-dependent particle loss in the UHSAS inlet line: super-micron particles are subject to enhanced inertial impaction at bends and fittings, gravitational settling in horizontal sections, and turbulent deposition along internal surfaces. The losses scale strongly with particle size, becoming significant for diameters above a few hundred nanometers in plumbing not specifically designed for super-micron transport. This is a recognized deficiency of the standard UHSAS inlet design and is consistent with the progressive undercount observed here, which intensifies monotonically with increasing PSL size from 700 nm to 1 μm.

Overall, the UHSAS demonstrates excellent counting agreement with the leave-one-out reference for sub-700 nm PSL particles, consistent with its strong sub-micron sensitivity and high size resolution. The systematic undercount observed for PSL diameters of 700 nm and above is most plausibly attributable to particle losses in the inlet line rather than to an intrinsic limitation in the optical block's detection efficiency. For applications requiring quantitative counting of super-micron particles, the UHSAS results should either be inlet-loss-corrected (e.g., using a calibrated transmission curve) or supplemented by an instrument with a more transmissive coarse-mode inlet (such as the APS).

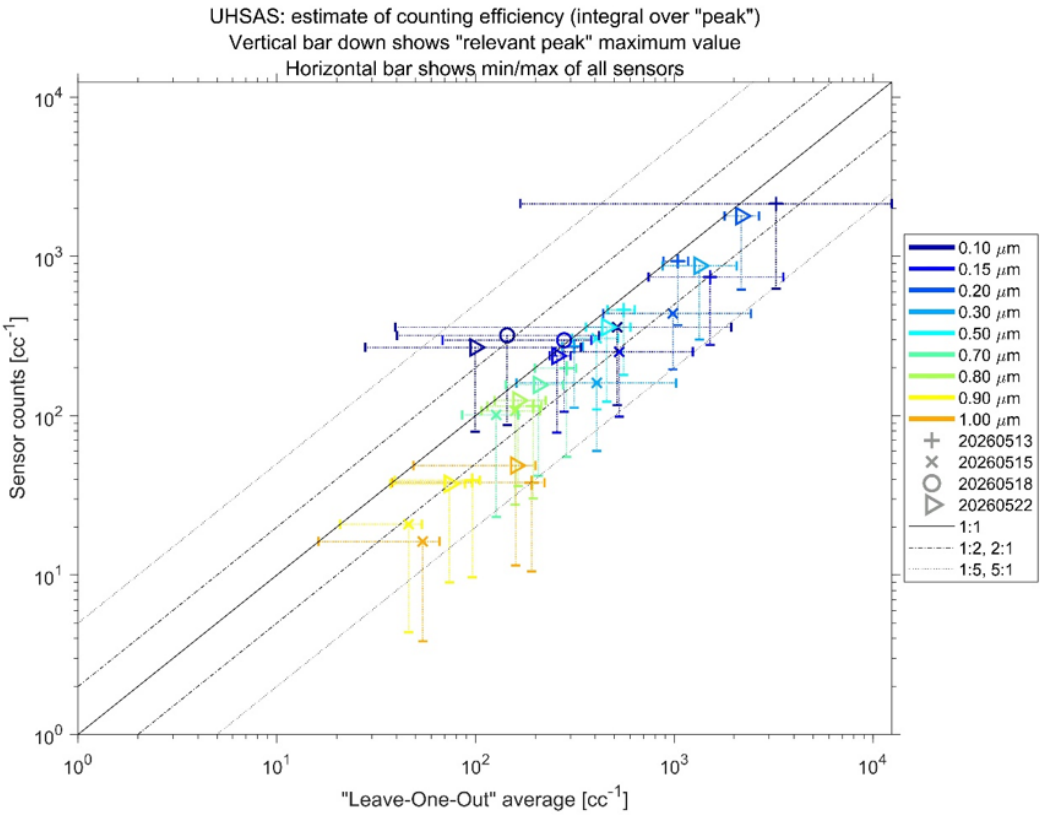


Figure 11. UHSAS counting efficiency: sensor-reported number concentration (integrated over the relevant peak window) versus the leave-one-out average concentration from all other co-located sensors that have the PSL size within their valid measurement range.

4.2.3 APS

Figure 12 shows the counting-efficiency response of the APS across its operational PSL test range (500 nm to 3 µm) for the four repeat experiments conducted on 13, 15, 18, and 22 May 2026. Data are not reported for PSL diameters below 500 nm, which are outside the APS detection range. The APS counting response exhibits a clear size-dependent pattern: the agreement with the leave-one-out reference is good at the largest sizes and at 500 nm, but a systematic undercount emerges in the intermediate 700–1000 nm range:

- **500 nm:** The APS markers cluster tightly around the 1:1 line, well within the 1:2/2:1 envelope. Day-to-day reproducibility across the four test markers is excellent. This agreement is notable given the systematic one-to-two-bin sizing offset documented for this size in Section 5.1 — the integrated counts within the relevant peak window remain consistent with the leave-one-out reference even though the reported peak diameter is biased low.
- **Intermediate range (700-1000 nm):** A systematic undercount develops, with markers falling below the 1:1 line and several measurements approaching or crossing the 1:5 envelope at 900 nm and 1 µm. The leave-one-out reference at these sizes is dominated by the POPS units and the PCASP, all of which agree within a factor of two with each other (per Section 5.1). The APS is therefore the discrepant sensor at the upper end of the sub-micron range, in contrast to its good agreement at 500 nm and at super-micron sizes.

- **Super-micron range (2-3 µm):** The APS markers return to good agreement with the leave-one-out reference, falling within the 1:2/2:1 envelope and clustering around the 1:1 line. This is the size range for which the APS is specifically optimized: the time-of-flight measurement principle delivers high counting efficiency for super-micron particles, and the inlet is engineered for efficient coarse-mode transmission. The wider relative scatter at 3 µm is consistent with counting-statistics noise at low absolute concentrations (typically < 1 cm^{-3}) rather than a systematic instrument bias.

The undercount in the 700-1000 nm range is consistent with the well-documented behavior of the APS 3321 in this size range, where two factors combine to reduce the effective counting efficiency. First, the time-of-flight detection efficiency of the APS is known to decline below ~1 µm, with reported detection efficiencies dropping substantially in the 0.7-1.0 µm range as the time-of-flight signal-to-noise degrades and the inversion algorithm becomes less reliable. Second, the systematic one-to-two-bin sizing offset documented in Section 4.1.3 places the measured peak in a different bin range than the leave-one-out reference would predict, and the broadened, asymmetric peaks in this range can extend across more bins than the relevant peak window captures, leading to additional integration losses. The combined effect is the observed undercount of up to a factor of five at 900 nm-1 µm.

The wide vertical error bars at 700-1000 nm reflect both the broadened, asymmetric peak shapes characteristic of the APS in this range and the long downward tail produced when a low-count peak bin is integrated alongside neighboring near-zero bins. This is a feature of the peak-integration definition combined with the APS response in its lower size range, not an indication of measurement instability — the marker positions remain reproducible across the four test days.

Overall, the APS demonstrates excellent counting agreement with the leave-one-out reference in its design-optimized super-micron range (2-3 µm) and at 500 nm, but substantially undercounts in the 700-1000 nm transition region, where its detection efficiency declines and its sizing response broadens. This complementary size dependence relative to the UHSAS — which performs well at sub-700 nm but undercounts above — illustrates a key result of this study: no single instrument provides quantitative counting across the full sub- to super-micron range, and a composite size distribution drawing on each instrument's optimal range is required for accurate ensemble characterization.

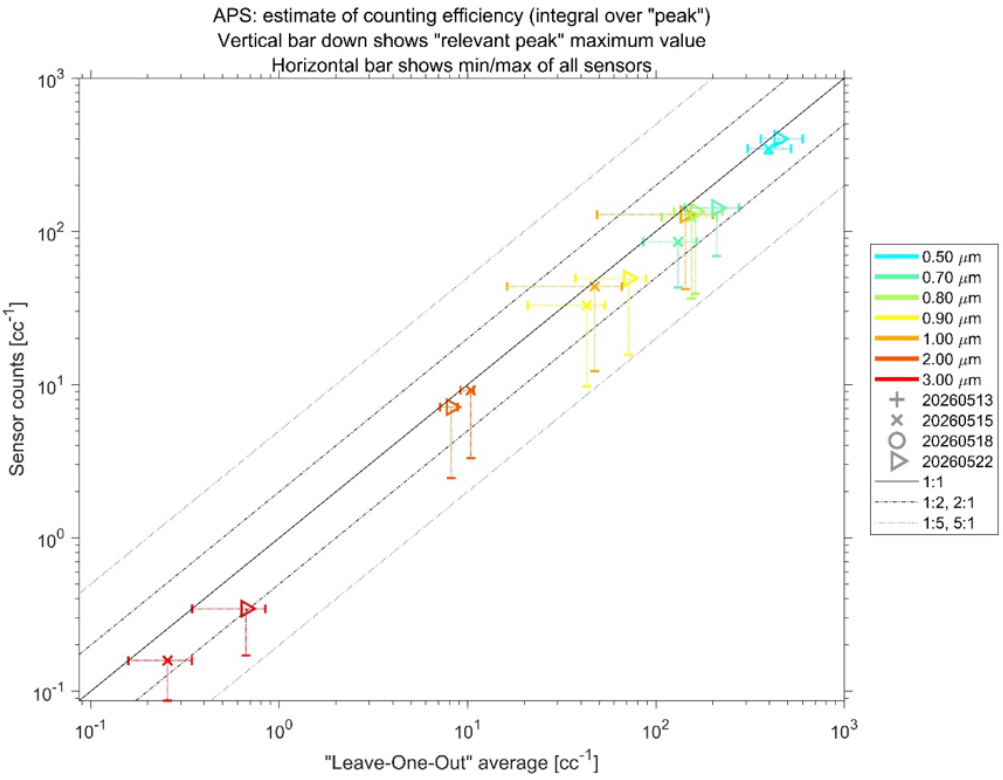


Figure 12. APS counting efficiency: sensor-reported number concentration (integrated over the relevant peak window) versus the leave-one-out average concentration from all other co-located sensors that have the PSL size within their valid measurement range.

4.2.4 PCASP

Figure 13 shows the counting-efficiency response of PCASP across the full PSL test range (100 nm to 3 μm) for the four repeat experiments conducted on 13, 15, 18, and 22 May 2026. Across most of the test range, the PCASP tracks the leave-one-out reference within a factor of two, demonstrating reasonable counting agreement with the ensemble of co-located sensors. Several size-dependent features are observed:

- **Sub-200 nm range (100 nm and 150 nm):** The counting efficiency is significantly reduced. The 100 nm and 150 nm markers consistently fall below the 1:1 line, with several points lying near or beyond the 1:5 envelope. This behavior is consistent with operation near the lower detection limit of the PCASP (~100 nm), where the detection efficiency curve is rising steeply but has not yet reached unity. At these sizes, the leave-one-out reference is limited to UHSAS, so the PCASP appears to undercount relative to the more sensitive instruments. SMPS was excluded due to data-reduction issues with the multiply-charge correction. The very wide horizontal error bars at 100 nm also reflect substantial sensor-to-sensor disagreement among the contributing instruments at this challenging size, magnifying the apparent scatter.
- **Mid-range (200-500 nm):** The markers cluster close to the 1:1 line, generally within the 1:2/2:1 envelope. The PCASP works well within its specified operational range here, and the counting agreement with the leave-one-out reference is good. Day-to-day reproducibility across the four test markers is also strong.

- **Mie-resonance region (700-1000 nm):** Counts continue to track the 1:1 line within a factor of two. As noted in the sizing-accuracy analysis (Section 4.1.4), the coarse bin structure of the PCASP produces wide peak-integration windows in this range, which tends to capture the full PSL peak even where Mie-resonance ambiguity is present. The counting agreement therefore remains good despite the reduced size resolution.
- **Super-micron range (2-3 µm):** Although the absolute concentrations are very low (typically <10 cm^{-3}), the PCASP tracks the leave-one-out reference within a factor of two, with the four test days clustering tightly around the 1:1 line. The wider relative scatter at 3 µm is consistent with counting-statistics noise at low concentrations rather than a systematic instrument bias.

Note that the wide error bars associated with the PCASP measurements — particularly at sub-300 nm sizes — primarily reflect the instrument's coarse bin structure and the resulting sensitivity of the integrated counts to peak-window placement, rather than measurement instability. The marker positions are reproducible across the four test days, indicating that the PCASP responds consistently to a given PSL challenge; its limitation lies in the coarse spectral resolution of the reported response, not in the stability of the measurement.

Overall, the PCASP demonstrates good counting agreement with the leave-one-out reference across its specified operating range, with a clear and physically expected reduction in counting efficiency below ~200 nm associated with its lower detection limit. For applications targeting particles below ~200 nm, the PCASP data should be supplemented by a sensor with higher sub-200 nm sensitivity (such as the UHSAS).

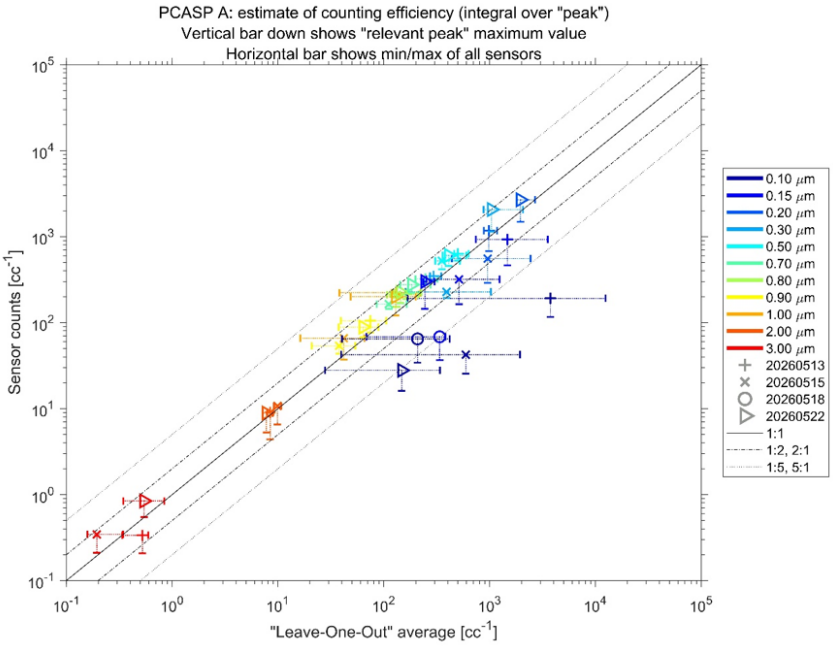


Figure 13. PCASP counting efficiency: sensor-reported number concentration (integrated over the relevant peak window) versus the leave-one-out average concentration from all other co-located sensors that have the PSL size within their valid measurement range.

4.2.5 SMPS

Figure 14 shows the counting-efficiency response of the SMPS across its accessible PSL test range (100 nm to 300 nm) for the four repeat experiments conducted on 13, 15, 18, and 22 May 2026. As discussed in Section 4.1.5, PSL diameters above 300 nm are not accessible to the SMPS in this experiment owing to the flow-balance constraints imposed by the 2.5 LPM atomizer aerosol flow.

In contrast to the excellent sizing accuracy demonstrated by the SMPS in Section 4.1.5, the counting efficiency results show systematic disagreement with the leave-one-out reference. The SMPS markers consistently lie *above* the 1:1 line across all four PSL sizes, with the overcount typically falling between the 1:2/2:1 and 1:5/5:1 envelopes. The wide horizontal error bars across all sizes indicate substantial sensor-to-sensor disagreement among the contributing instruments in the leave-one-out reference, particularly at 100 nm and 150 nm where the UHSAS is the only other fully-in-range sensor and the POPS and PCASP contribute only partial counts owing to their lower-detection-limit behavior (Sections 4.2.1 and 4.2.4). The reference itself is therefore noisy at these sizes, which contributes some scatter to the SMPS-versus-leave-one-out comparison; however, the *direction* of the SMPS bias (consistently high) cannot be explained by reference noise alone.

Likely cause: incomplete multiple-charge correction in the data reduction. The systematic overcount is most plausibly attributable to an issue in the SMPS data reduction pipeline, specifically the multiple-charge correction. When PSL particles are atomized, residual material from the suspension liquid produces a broad sub-200 nm aerosol that is then charge-conditioned in the SMPS neutralizer. The bipolar charge distribution places a non-negligible fraction of larger particles into doubly- and triply-charged states, which then pass through the DMA at a smaller apparent (mobility-equivalent) diameter than their physical diameter. A correctly implemented multiple-charge correction algorithm uses the measured size distribution at larger diameters to estimate and subtract these multiply-charged contributions from the smaller-size bins, recovering the true singly-charged size distribution.

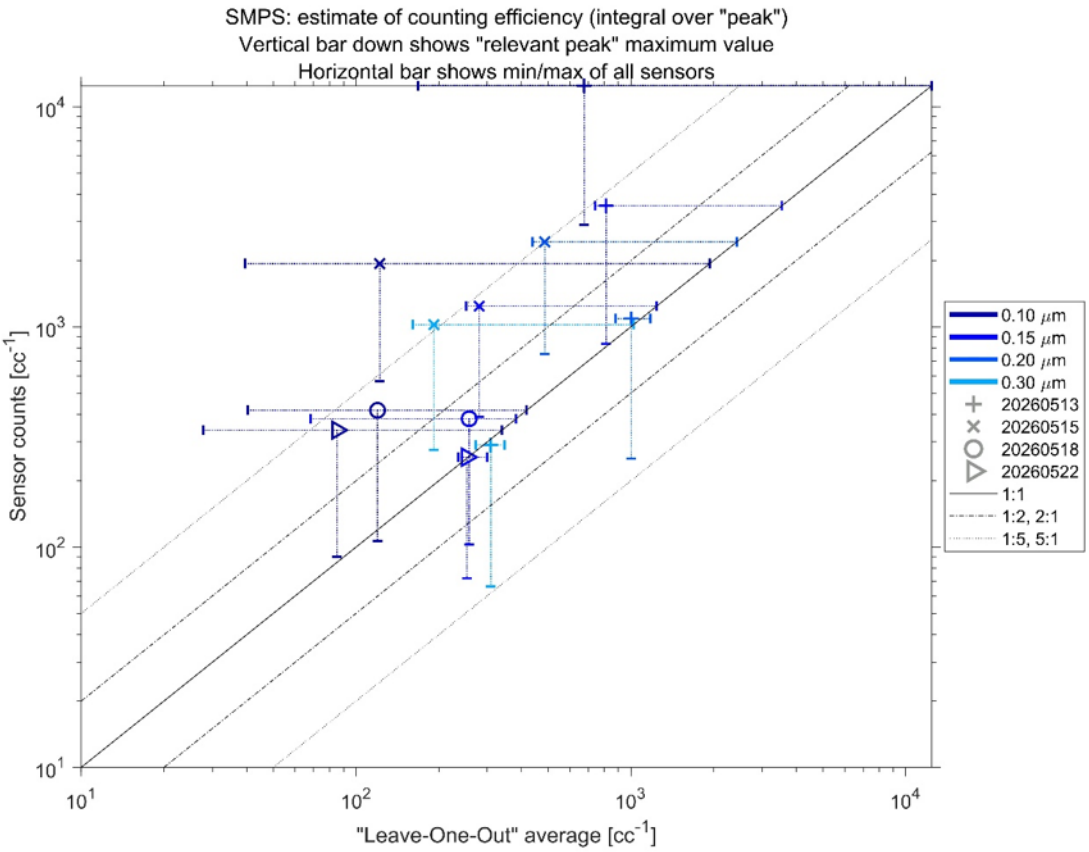


Figure 14. SMPS counting efficiency: sensor-reported number concentration (integrated over the relevant peak window) versus the leave-one-out average concentration from all other co-located sensors that have the PSL size within their valid measurement range.

5.0 Summary

This report presents a comparative evaluation of seven co-located aerosol size-distribution sensors — three POPS units (POPS269, POPS308, POPS434), one UHSAS, one APS, one PCASP, and one SMPS — challenged with monodisperse PSL particles spanning 100 nm to 3 µm. The smallest two sizes (100 nm and 150 nm) were generated via DMA classification, and the remaining sizes were produced from certified PSL suspensions. Four repeat experiments were conducted on 13, 15, 18, and 22 May 2026 to assess day-to-day reproducibility. Two performance metrics were evaluated for each instrument: (1) sizing accuracy, by comparing the measured peak diameter to the nominal PSL diameter, and (2) counting efficiency, by comparing the sensor-reported integrated number concentration to a leave-one-out reference computed from the remaining co-located sensors that have the PSL size within their valid measurement range.

Key findings are set out below.

5.1 Sizing Accuracy

- **POPS units (×3):** All three POPS units agree with the nominal PSL diameter to within ±20% across nearly the entire test range, and to within ±10% for most sizes between 200 nm and 2 μm. Reported peak diameters lie slightly above the 1:1 line near the lower detection limit (~135 nm), consistent with coarse bin resolution at the limit, and a modest underestimation is observed in the Mie-resonance region (~700-1000 nm versus 405 nm laser wavelength).
- **UHSAS:** Demonstrates the best sizing accuracy of the optical instruments tested, with measurements within ±10% of nominal across its full operational range (100 nm-1 μm). Minor deviations near 1 μm reflect the onset of Mie-resonance ambiguity as particles approach the 1054 nm laser wavelength.
- **APS:** Reports diameters that are systematically biased low by approximately one to two bins (~10–20%) across its full operating range (500 nm-3 μm). Day-to-day reproducibility is excellent, but the consistent offset suggests a calibration or bin-edge assignment issue rather than a physical density effect. Most probably, this deficiency will be corrected with the next maintenance service/calibration.
- **PCASP:** Shows reasonable sizing accuracy (within ±20% of nominal across the test range) and good day-to-day reproducibility, but with wide error bars reflecting the instrument's coarse bin structure rather than measurement noise.
- **SMPS:** Provides the most accurate and reproducible sizing of all instruments tested, with all measurements within ±10% of nominal. The accessible range is restricted to ≤300 nm in this experiment by flow-balance constraints arising from the 2.5 LPM atomizer aerosol flow.

5.2 Counting Efficiency

- **POPS units (×3):** Track the leave-one-out reference within a factor of two across most of the test range. A clear, physically expected loss of counting efficiency below ~150 nm is associated with the ~135 nm lower detection limit; at 100 nm the particles fall below the detection threshold and only a small fraction is registered, while at 150 nm the detection efficiency is rising steeply but has not yet reached unity.
- **UHSAS:** Excellent agreement with the leave-one-out reference for sub-700 nm particles, but a progressive systematic undercount develops above 700 nm, getting beyond the 1:5 envelope at 900 nm-1 μm. The size-dependent pattern, combined with the preserved sizing accuracy in the same range, points to size-dependent particle losses in the inlet line as the dominant mechanism — a design limitation of the standard UHSAS inlet size and geometry.
- **APS:** Excellent counting agreement in the design-optimized super-micron range (2-3 μm) and at 500 nm, but a substantial undercount in the 700-1000 nm transition region, where the time-of-flight detection efficiency declines and the inversion-algorithm response broadens. The size-driven nature of the undercount is supported by ruling out coincidence (high-concentration) and counting-statistics (low-concentration) failure modes; concentration may modulate the visibility of the effect but does not drive it.
- **PCASP:** Reasonable counting agreement within a factor of two across the operating range, with a clear, physically expected reduction below ~200 nm associated with the lower detection limit. Wide error bars reflect coarse bin structure rather than measurement instability.

- **SMPS:** Counting results are anomalous — the SMPS systematically *overcounts* relative to the leave-one-out reference across all four accessible PSL sizes (100-300 nm), with the overcount largest at the smallest sizes. The direction, size dependence, and reproducibility of this bias, combined with the otherwise excellent sizing performance, point to an issue in the data reduction pipeline — most likely an incorrectly applied or misleading multiple-charge correction. SMPS counting results should therefore be regarded as **provisional** pending verification.

5.3 Inter-POPS Reproducibility

- The three POPS units show near-complete overlap at every PSL size across the full test range, typically within a factor of two and often within the symbol size, across nearly four orders of magnitude in concentration. No systematic offset is apparent between any pair of units, supporting their treatment as a consistent ensemble for multi-sensor deployments without unit-specific correction factors.

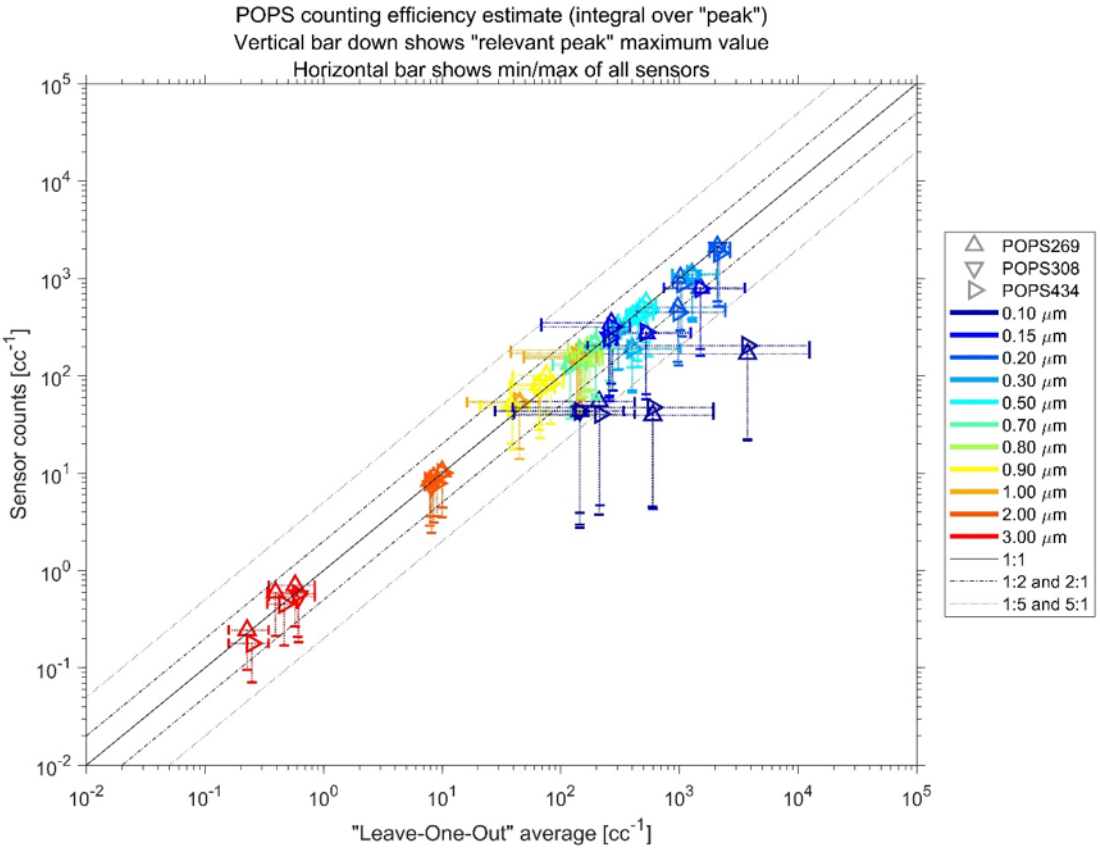


Figure 15. All POPS counting efficiency: sensor-reported number concentration (integrated over the relevant peak window) versus the leave-one-out average concentration from all other co-located sensors that have the PSL size within their valid measurement range.

5.4 Cross-Instrument Implication

A key result of this study is that the UHSAS and APS exhibit complementary size-dependent counting performance: the UHSAS performs well below ~700 nm but undercounts above, while the APS performs well above ~2 μm but undercounts in the 700-1000 nm transition. No single instrument provides quantitative counting across the full sub- to super-micron range; a composite size distribution drawing on each instrument's optimal range is required for accurate ensemble characterization.

6.0 Lessons Learned and Recommendations for Future Deployments

This intercomparison demonstrated that aerosol size-distribution instruments should be evaluated within their valid measurement domains before quantitative comparison. Instruments based on optical scattering, aerodynamic time-of-flight, and electrical mobility do not report identical diameter definitions, and direct comparison requires careful interpretation. Repeated PSL challenges showed that sizing accuracy and counting efficiency are distinct performance metrics; both are needed to evaluate deployment readiness. The POPS instruments showed generally good sizing agreement across much of the tested range, while near-limit optical sizing and Mie-resonance regions require caution. The UHSAS results indicate that inlet transmission losses can significantly affect coarse-particle counting and should be characterized before field deployment. The APS results suggest that systematic bin offsets should be investigated through additional calibration checks. Overall, future deployments should include pre-deployment PSL validation, documented inlet-loss corrections, clear valid-range definitions, and standardized uncertainty reporting.

- Verify and correct the SMPS multiple-charge correction algorithm. Re-examine the data reduction pipeline to confirm that the multiple-charge correction is enabled, algorithm corresponds to used neutralizer type (X-ray or rad-based), applied over a sufficient size range to capture doubly- and triply-charged contributions, and configured with an appropriate DMA transfer function and bipolar charge distribution model for the sheath-to-aerosol flow ratio used. Reprocess and revisit Section 4.2.5 once corrected.
- Quantify and apply UHSAS inlet-loss corrections. Develop a calibrated transmission curve for the UHSAS inlet line — ideally derived from co-located coarse-mode references such as the APS and POPS — to enable inlet-loss correction of UHSAS counts above 700 nm. Consider hardware modifications to the UHSAS inlet design for future deployments requiring quantitative counting near 1 μm.
- Investigate the APS one-to-two-bin sizing offset. Conduct a follow-up calibration check with PSL standards covering the 500 nm-3 μm range to determine whether the offset originates in the time-of-flight calibration or the bin-edge assignment. Document the offset and apply a correction factor for cross-instrument analyses where APS-reported diameters are compared directly to optical or mobility-based measurements.

7.0 References

Johnson, TJ, M Irwin, JP Symonds, JS Olfert, and AM Boies. 2018. "Measuring aerosol size distributions with the aerodynamic aerosol classifier." *Aerosol Science and Technology* 52(6): 655–665, https://doi.org/10.1080/02786826.2018.1440063

Kupc, A, C Williamson, NL Wagner, M Richardson, and CA Brock. 2018. "Modification, calibration, and performance of the Ultra-High Sensitivity Aerosol Spectrometer for particle size distribution and volatility measurements during the Atmospheric Tomography Mission (ATom) airborne campaign." *Atmospheric Measurement Techniques* 11(1): 369–383, https://doi.org/10.5194/amt-11-369-2018

Mei, F, G McMeeking, M Pekour, RS Gao, G Kulkarni, S China, H Telg, D Dexheimer, J Tomlinson, and B Schmid. 2020. "Performance Assessment of Portable Optical Particle Spectrometer (POPS)." *Sensors* 20(21), https://doi.org/10.3390/s20216294

Reid, JS, HH Jonsson, HB Maring, A Smirnov, DL Savoie, SS Cliff, EA Reid, JM Livingston, MM Meier, O Dubovik, and S-C Tsay. 2003. "Comparison of size and morphological measurements of coarse mode dust particles from Africa." *Journal of Geophysical Research – Atmospheres* 108(D19): 8593, https://doi.org/https://doi.org/10.1029/2002JD002485

Seinfeld, JH, and SN Pandis. 2016. *Atmospheric Chemistry and Physics: From Air Pollution to Climate Change*. (3rd Edition) John Wiley & Sons, Hoboken, New Jersey.

Stolzenburg, MR. 1988. An ultrafine aerosol size distribution measuring system. PhD Dissertation, University of Minnesota.

Wu, T, and BE Boor. 2021. "Urban aerosol size distributions: a global perspective." *Atmospheric Chemistry and Physics* 21(11): 8883–8914, https://doi.org/10.5194/acp-21-8883-2021



www.arm.gov

U.S. DEPARTMENT OF
ENERGY

Office of Science